MASS CONSTRAINTS OF THE WASP-47 PLANETARY SYSTEM FROM RADIAL VELOCITIES

Evan Sinukoff[1,14], Andrew W. Howard[2], Erik A. Petigura[3,15], Benjamin J. Fulton[1,16], Howard Isaacson[4], Lauren M. Weiss[5], John M. Brewer[6], Brad M. S. Hansen[7], Lea Hirsch[4], Jessie L. Christiansen[8], Justin R. Crepp[9], Ian J. M. Crossfield[10,17], Joshua E. Schlieder[8,18], David R. Ciardi[8], Charles A. Beichman[8], Heather A. Knutson[3], Bjoern Benneke[3], Courtney D. Dressing[3,17], John H. Livingston[11], Katherine M. Deck[3], Sébastien Lépine[12] Leslie A. Rogers[13]

Draft version December 16, 2016

ABSTRACT

We report precise radial velocity (RV) measurements of WASP-47, a G star that hosts three transiting planets in close proximity (a hot Jupiter, a super-Earth and a Neptune-sized planet) and a non-transiting planet at 1.4 AU. Through a joint analysis of previously published RVs and our own Keck-HIRES RVs, we significantly improve the planet mass and bulk density measurements. For the super-Earth WASP-47e ($P = 0.79$ days), we measure a mass of $9.11 \pm 1.17\,M_\oplus$, and a bulk density of $7.63 \pm 1.90\,\mathrm{g\,cm^{-3}}$, consistent with a rocky composition. For the hot Jupiter WASP-47b ($P = 4.2$ days), we measure a mass of $356 \pm 12\,M_\oplus$ ($1.12 \pm 0.04\,M_{\mathrm{Jup}}$) and constrain its eccentricity to < 0.021 at 3-σ confidence. For the Neptune-size planet WASP-47d ($P = 9.0$ days), we measure a mass of $12.75 \pm 2.70\,M_\oplus$, and a bulk density of $1.36 \pm 0.42\,\mathrm{g\,cm^{-3}}$, suggesting it has a thick H/He envelope. For the outer non-transiting planet, we measure a minimum mass of $411 \pm 18\,M_\oplus$ ($1.29 \pm 0.06\,M_{\mathrm{Jup}}$), an orbital period of 595.7 ± 5.0 days, and an orbital eccentricity of 0.27 ± 0.04. Our new measurements are consistent with but 2–4× more precise than previous mass measurements.

1. INTRODUCTION

Approximately 1% of Sun-like stars host giant planets on short-period orbits (P < 10 days), known as hot Jupiters (HJs, Howard et al. 2012; Wright et al. 2012). These planets are thought to have migrated to their observed locations from beyond the ice-line at several AU. One proposed migration mechanism involves dynamical interaction between the planet and protoplanetary disk

[1] Institute for Astronomy, University of Hawai'i at Mānoa, Honolulu, HI 96822, USA
[2] Cahill Center for Astrophysics, California Institute of Technology, 1216 East California Boulevard, Pasadena, CA 91125, USA
[3] Division of Geological and Planetary Sciences, California Institute of Technology, 1255 East California Blvd, Pasadena, CA 91125, USA
[4] Astronomy Department, University of California, Berkeley, CA, USA
[5] Institut de Recherche sur les Exoplanètes, Dèpartement de Physique, Universitè de Montrèal, C.P. 6128, Succ. Centre-ville, Montréal, QC H3C 3J7, Canada
[6] Department of Astronomy, Yale University and 260 Whitney Avenue, New Haven, CT 06511, USA
[7] Department of Physics & Astronomy and Institute of Geophysics & Planetary Physics, University of California Los Angeles, Los Angeles, CA 90095, USA
[8] NASA Exoplanet Science Institute, California Institute of Technology, 770 S. Wilson Ave., Pasadena, CA, USA
[9] Department of Physics, University of Notre Dame, 225 Nieuwland Science Hall, Notre Dame, IN, USA
[10] Department of Astronomy & Astrophysics, University of California Santa Cruz, 1156 High St., Santa Cruz, CA, USA
[11] Department of Astronomy, The University of Tokyo, 7-3-1 Bunkyo-ku, Tokyo 113-0033, Japan
[12] Department of Physics and Astronomy, Georgia State University, GA, USA
[13] Department of Astronomy & Astrophysics, University of Chicago, 5640 South Ellis Avenue, Chicago, IL 60637, USA
[14] NSERC Postgraduate Research Fellow
[15] Hubble Fellow
[16] NSF Graduate Research Fellow
[17] NASA Sagan Fellow
[18] NASA Postdoctoral Program Fellow

(e.g. Lin et al. 1996). In this case, the planet maintains a low eccentricity. Other "high-eccentricity migration" (HEM) modes have been proposed including planet-planet scattering (e.g. Rasio & Ford 1996), Kozai oscillations induced by either a nearby star (e.g. Wu & Murray 2003) or planet (e.g. Naoz et al. 2011), and secular interactions (e.g. Wu & Lithwick 2011). In the HEM scenario, gravitational perturbations excite planets onto eccentric orbits, which subsequently shrink and circularize due to stellar tides. Other proposed dynamical effects include misalignment between the orbital axis of the HJ and the stellar spin axis, as well as the destabilization of close-in planets encountered upon migration.

Observations of systems with HJs are difficult to reconcile with HEM theory. For example, Schlaufman & Winn (2016) found that HJ host stars are no more likely to host additional giant planets than stars with giant planets at $P > 10$ days. Knutson et al. (2014) found no difference between the occurrence of additional giant planets at 1–20 AU in systems with HJs whose orbits are eccentric or misaligned versus circular and aligned with the stellar spin. Moreover, Dawson et al. (2015) concluded that the number of migrating Jupiters on highly eccentric orbits is lower than predicted by HEM theory (Socrates et al. 2012).

In support of HEM theory, Steffen et al. (2012) found an absence of HJs in close proximity to smaller planets (0.7–$5\,R_\oplus$) discovered by *Kepler*. However, it remains unclear whether HJs are intrinsically lonely or if their close neighbors have merely evaded detection. For example, Batygin et al. (2016) proposed a mechanism for in-situ formation of HJs, which predicts a population of small planets mutually inclined to the HJ, and therefore unlikely to transit. While HJs are observed to be lonely, Huang et al. (2016) found that roughly half of transiting "warm-Jupiters" ($P = 10$–200 days) are accompanied by transiting planets ~ 2–$6\,R_\oplus$ on interior orbits $P < 50$

days. They proposed that the warm-Jupiters in these multi-planet systems formed in-situ and that occasionally this same mechanism might produce a very small fraction of HJs. These latest theories add to the diversity of theories to explain HJ formation.

WASP-47 is the first star known to host a Jovian-size planet with $P < 10$ days and additional close-in planets—proof that not all HJs are isolated and strengthening the argument that HEM alone cannot produce the entire population of HJs. The Jovian-size planet WASP-47b orbits the star every 4.2 days. It was first reported and confirmed by Hellier et al. (2012) who detected both its transit and radial velocity (RV) signatures. Becker et al. (2015) detected two additional transiting planets using $K2$ photometry. One of these planets, WASP-47e, is an ultra-short-period (USP) super-Earth ($P = 0.79$ days). WASP-47d is Neptune-size ($P = 9.0$ days). Becker et al. (2015) detected transit timing variations (TTVs) of both planets. Their TTV signals are anticorrelated and have a super-period consistent with 52.67-days — the expected super-period for two such planets near 2:1 orbital mean-motion-resonance (Lithwick et al. 2012). Becker et al. (2015) reported planet mass constraints $M_b = 341^{+73}_{-55}\,M_\oplus$, $M_d = 15.2 \pm 7\,M_\oplus$, and $M_e < 22\,M_\oplus$ based on dynamical fits to the observed transit times. Measurements of the Rossiter-McLaughlin effect by (Sanchis-Ojeda et al. 2015) ruled out orbits that are strongly misaligned with the stellar spin axis. Crossfield et al. (2016) independently validated the planetary system by demonstrating that the star is unlikely to be a blend of multiple stars, via Keck-NIRC2 adaptive optics images and a search for secondary lines in the stellar spectrum.

A fourth planet, WASP-47c, was detected with an orbital period of 572 ± 7 days by Neveu-VanMalle et al. (2016) from 32 RV observations with the Euler/CORALIE instrument spanning almost 3 years[19]. Neveu-VanMalle et al. (2016) measure a minimum mass $M_c \sin i = 394 \pm 70\,M_\oplus$. WASP-47c joins the population of giant planets beyond 1 AU that have been found in systems with HJs (Knutson et al. 2014).

WASP-47d and WASP-47e are examples of super-Earth- and Neptune-size planets, which are common around Sun-like stars (Howard et al. 2012; Fressin et al. 2013; Petigura et al. 2013; Burke et al. 2015). Only a handful of these planets have precisely measured masses and bulk densities. Compositional trends have emerged from this limited sample. Planets smaller than $\approx 1.6\,R_\oplus$ typically have high densities consistent with Earth-like bulk compositions, while most larger planets have low densities that require thick envelopes of H/He (Weiss & Marcy 2014; Marcy et al. 2014; Lopez & Fortney 2014; Rogers 2015; Dressing et al. 2015). However, there is significant scatter about the mean mass-radius relationship, indicating compositional diversity, even for a fixed planet radius. Due to the limited number of known sub-Neptunes with bright host stars, mass measurements are scarce, and this compositional diversity has yet to be fully explored.

Dai et al. (2015) obtained 26 RVs of WASP-47 with the

Carnegie Planet Finder Spectrograph (PFS), measuring $M_b = 370 \pm 29\,M_\oplus$, $M_e = 12.2 \pm 3.7\,M_\oplus$, and $M_d = 10.4 \pm 8.4\,M_\oplus$, consistent with TTV measurements by Becker et al. (2015). Dai et al. (2015) measure a bulk density of WASP-47e of $11.2 \pm 3.6\,\mathrm{g\,cm^{-3}}$, consistent with a rocky and potentially iron-rich composition. Their $\sim 80\%$ measurement uncertainty on the mass of planet d is insufficient to constrain the planet's bulk composition.

Here we present improved mass constraints of all four planets in the WASP-47 system by combining Keck-HIRES RVs with the previously published RVs of Hellier et al. (2012), Dai et al. (2015), and Neveu-VanMalle et al. (2016). This work is part of a NASA "Key Project" to measure $K2$ planet masses using Keck-HIRES. Section 2 of this manuscript summarizes our Doppler observations and spectroscopic constraints of stellar parameters. Our analysis of the RV time-series and resulting planet mass measurements are detailed in Section 3. In Section 4, we discuss possible compositions of WASP-47e and WASP-47d, eccentricity constraints of the Hot-Jupiter, and interpret these in the context of planet formation and evolution.

2. OBSERVATIONS

2.1. K2 Photometry

WASP-47 was observed by the Kepler Telescope for 69 consecutive days in Campaign 3 (C3) of NASA's $K2$ mission (Howell et al. 2014). It was one of only 55 targets in $K2$ Campaign 3 that was observed in short-cadence mode (60 sec), enabling precise measurement of transit parameters. We adopt the orbital ephemerides, and transit depths reported by Becker et al. (2015).

2.2. Radial Velocity Measurements

We collected RV measurements of WASP-47 using HIRES (Vogt et al. 1994) at the W. M. Keck Observatory from 2015 August 10 UT to 2016 October 7 UT (424 days). We followed standard procedures of the California Planet Search (CPS; Howard et al. 2010). For each RV observation, we used the "C2" decker ($0''.87 \times 14''$ slit), which yields a spectral resolution $R = 55,000$ and is long enough for sky subtraction. Before the starlight entered the spectrometer slit, it first passed through a cell of iodine gas, which imprints a dense set of molecular absorption lines on the stellar spectrum. These iodine lines were used for wavelength calibration and PSF reference. We used an exposure meter to terminate exposures after reaching a SNR per pixel of ~ 100 at $550\,\mathrm{nm}$ (typically ~ 15 min). A single iodine-free spectrum was obtained as a stellar template using the "B3" decker ($0''.57 \times 14''$ slit). RVs were measured by forward modeling each observed spectrum as the product of an RV-shifted iodine-free spectrum and a high-resolution/high-SNR iodine transmission spectrum. The latter was first convolved with an instrumental PSF, modeled as the sum of 13 Gaussians with fixed centers and widths but variable amplitudes (Marcy & Butler 1992; Valenti et al. 1995; Butler et al. 1996; Howard et al. 2009). Our measured RVs are listed in Table 3.

2.3. Stellar Parameters

We measured the effective temperature (T_{eff}), surface gravity ($\log g$), and metallicity ([Fe/H]) of WASP-47

---

[19] WASP-47d and WASP-47e were published before WASP-47c, which was named while the work of Neveu-VanMalle et al. (2016) was still under revision.

TABLE 1
RV DATASETS

Reference[a]	Instrument	N_{RV}	Median Unc. [m s^{-1}]	Δt [days]
This study	HIRES	47[b]	1.8	424
V16	CORALIE	26	11.4	745
D15	PFS	26	3.1	12
H12	CORALIE	19	11.0	560

[a] V16: Neveu-VanMalle et al. (2016), D15: Dai et al. (2015), H12: Hellier et al. (2012)

[b] We made 74 RV measurements with Keck-HIRES, but omit 17 RVs measured during the WASP-47b transit event on 2015 August 10 UT. We binned the remaining 12 RVs from that night into two measurements for a total of 47 RVs

from our iodine-free HIRES spectrum using the updated SME analysis of Brewer et al. (2016). This new methodology yields $\log g$ values that are accurate to 0.05 dex, as determined from careful comparisons against stars with $\log g$ determined from asteroseismology (Brewer et al. 2015). We find $T_{eff} = 5475\pm60$ K, $\log g = 4.27\pm0.05$ dex, and [Fe/H] $= 0.36 \pm 0.05$ dex. To estimate the stellar mass and radius, we fit our spectroscopic measurements of T_{eff}, $\log g$, & [Fe/H] to a grid of models from the Dartmouth Stellar Evolution Database (Dotter et al. 2008) using the `isochrones` Python package (Morton 2015) with uncertainties determined by the `emcee` Markov Chain Monte Carlo (MCMC) package (Foreman-Mackey et al. 2013). The derived stellar mass and radius are $0.99 \pm 0.03\,M_\odot$ and $1.18 \pm 0.08\,R_\odot$. These are consistent with the measurements of $1.04 \pm 0.08\,M_\odot$ and $1.15 \pm 0.04\,R_\oplus$ by Mortier et al. (2013). Following Sinukoff et al. (2016), we conservatively adopt uncertainties of 5% on stellar mass to account for the intrinsic uncertainties of the Dartmouth models estimated by Feiden & Chaboyer (2012).

Following the prescription of Isaacson & Fischer (2010), we measure S_{HK} indices from the HIRES spectra, which serve as a proxy for stellar activity. Our S_{HK} measurements are listed in Table 3. The median S_{HK} index of 0.132 is consistent with other inactive stars in the California Planet Search (Isaacson & Fischer 2010). Consistent with this picture, we measure the stellar jitter to be 3.7 ± 0.6 m s^{-1} (Table 2).

3. ANALYSIS

3.1. *Radial Velocity Data Analysis*

We analyzed the RV time-series using the RV fitting package `RadVel` (Fulton & Petigura, in prep.), which is publicly-available on GitHub[20]. We fit our Keck-HIRES RVs along with previously published RV datasets (Hellier et al. 2012; Dai et al. 2015; Neveu-VanMalle et al. 2016), summarized in Table 1. We omit the six RV measurements reported by Neveu-VanMalle et al. (2016) that were taken after a CORALIE instrument upgrade. These would have added two free parameters to our RV model, which was not worth the negligible gain in RV measurements. After omitting the 17 HIRES observations JD = 2457244.9366–2457245.07451, taken during a WASP-47b transit, we still have 12 out-of-transit observations from that night. RVs have astrophysical and instrumental er-

[20] https://github.com/California-Planet-Search/radvel http://radvel.readthedocs.io/en/master/index.html

rors that manifest on a variety of timescales from minutes to year. Therefore, the consecutive measurements during the same night don't constitute independent measurements. To guard against these data from having a disproportionate influence influence on the fit, we bin the 8 pre-transit RV measurements and bin the 4 post-transit measurements. We note that an analysis of our HIRES RVs alone gives the same planet masses to within 1σ.

We adopt a four-planet model that is the sum of four Keplerian components. For each of the four datasets, our model includes an RV offset, γ, as well as an RV "jitter" parameter, σ_{jit}, to account for additional Doppler noise of astrophysical or instrumental origins.

Our likelihood function for this analysis follows that of Howard et al. (2014):

$$\ln\mathcal{L} = -\sum_i \left[\frac{(v_i - v_m(t_i))^2}{2\left(\sigma_i^2 + \sigma_{jit}^2\right)} + \ln\sqrt{2\pi\left(\sigma_i^2 + \sigma_{jit}^2\right)} \right], \quad (1)$$

where v_i and σ_i are the ith RV measurement and corresponding uncertainty, and $v_m(t_i)$ is the Keplerian model velocity at time t_i. To increase the rate of convergence and to to counter the bias toward non-zero eccentricity (Lucy & Sweeney 1971), we adopt the following parametrization of our model RV curve: $\{P, T_c, \sqrt{e}\cos\omega, \sqrt{e}\sin\omega, K\}$, where P is orbital period, T_c is the time of conjunction, e is the orbital eccentricity, ω is the longitude of periastron and K is the RV semi-amplitude.

We first find the maximum-likelihood model using the minimization technique of Powell (1964), then perturb the best-fitting free parameters by up to 3% to start 100 parallel MCMC chains. The free parameters of the RV model are adopted as the MCMC step parameters. `RadVel` incorporates the affine-invariant sampler of the `emcee` package (Foreman-Mackey et al. 2013). The Gelman-Rubin (Gelman & Rubin 1992) and T_z statistics (Ford 2006) are checked in real-time during the MCMC exploration and the chains are deemed well-mixed and the MCMC run is halted when the Gelman-Rubin is within 3% of unity and $T_z > 1000$ for all free parameters.

We assume circular orbits for WASP-47d and WASP-47e while allowing the eccentricities of WASP-47b and WASP-47c to vary freely. An N-body dynamical stability analysis by Becker et al. (2015) showed that the orbits of the inner three planets are unstable when eccentricities of the three inner planets exceed ~ 0.05. For the ~ 4–6 m s^{-1} RV signals of WASP-47d and WASP-47e, our signal-to-noise is too low to distinguish between eccentricities of 0.00 and 0.05. The orbital periods and orbital phases of WASP-47b, d, and e were locked at the values reported in Becker et al. (2015) from transits. We adopt uninformed priors (i.e. no priors) on all free step parameters and step in linear parameter space. The median values and the 68% credible intervals are reported in Table 2. The best-fitting RV model is shown in Figure 1

We searched for additional companions at large or-

bital distances by testing RV models with and without a constant radial acceleration term, dv/dt. We compared these two models using the Bayesian Information Criterion (BIC), with the RV jitter fixed at the values in Table 2. We compute $\Delta\mathrm{BIC} = \mathrm{BIC}_{dv/dt} - \mathrm{BIC}_{dv/dt=0} = 3.8$, indicating that the simpler model is preferred, so we adopt $dv/dt = 0$.

We investigated whether the Keplerian orbit approximation is valid for our RV model, given the dynamical influences of the three inner planets on each other. First, we considered the TTV amplitudes, which indicate the order of magnitude of non-Keplerian effects. The TTV amplitudes of planets b, d, and e measured by Becker et al. (2015) of 0.63 min, 7.3 min, and < 1.2 min are 0.01%, 0.06%, and $< 0.1\%$ of the respective orbital periods. We assessed whether these deviations from Keplerian orbits are significant given the precision of our RV measurements. Given RV semi-amplitude K and assuming a phase shift equal to the TTV amplitude ΔT, the deviation of $\mathrm{RV}(t)$ is:

$$\Delta\mathrm{RV}(t) = \frac{\partial \mathrm{RV}}{\partial t}\Delta T$$
$$= \frac{2\pi K}{P}\cos\left(\frac{2\pi t}{P}\right)\Delta T. \tag{2}$$

The maximum $\Delta\mathrm{RV}$ is $2\pi K P^{-1}\Delta T$, which evaluates to $0.09\,\mathrm{m\,s^{-1}}$, $0.01\,\mathrm{m\,s^{-1}}$, and $< 0.03\,\mathrm{m\,s^{-1}}$ for planets b, d, and e respectively. These represent upper bounds to the orbit-averaged deviations from Keplerian over the K2 time baseline. These deviations are much smaller than our RV measurement uncertainties (1.5–2.0 m/s).

Since the RV time-series is much longer than the K2 baseline, one may wonder if there are large amplitude deviations from Keplerian orbits that build up over longer timescales. To verify that the TTVs remain small over the timescale of RV observations, we used the symplectic N-body integrator TTVFast (Deck et al. 2014) to numerically integrate the planet orbits over 2000 days. The orbital elements were initialized at the maximum-likelihood solution obtained from RVs. The TTV amplitudes of planets b, d, and e remained at 0.6 min, 7 min and < 1 min respectively over the 2000 day timespan.

We note that the orbital periods of planets b and d measured by Becker et al. (2015) do not accurately reflect the average orbital periods that would be measured over many years. Becker et al. (2015) measured P by fitting a linear ephemeris to the K2 transits. Since the K2 photometry only spans one TTV super-period, the Becker et al. (2015) orbital periods could be different from the average orbital periods over the time baseline of our RV measurements, which spans many TTV super-periods.

To quantify the additional uncertainties of average orbital periods, we used the 2000-day baseline of transit times obtained with TTVFast. For each planet, we performed a linear fit to every unique set of N consecutive transit times, where N is the number of transits observed in the K2 photometry. The resulting distribution of slopes (orbital periods) provides an estimate of the uncertainty of the average orbital period attributed to the limited timescale of K2 observations. The 1-sigma uncertainties obtained from these orbital period distributions are ± 0.000019 days and ± 0.00074 days for planets b and d respectively. These are $\sim 4\times$ larger than

the uncertainties reported by Becker et al. (2015). We refit our RV time-series using these larger orbital period uncertainties, but there was no change in the RV solution or corresponding uncertainties. The scale of these uncertainties is still a tiny fraction of the RV phase. Nevertheless we recommend that future studies adopt these larger uncertainties on average orbital period, which are listed in Table 2.

4. DISCUSSION

Figure 2 shows the mass-radius distribution of all confirmed planets with $R_p < 4.0\,R_\oplus$ whose mass and radius are measured to better than 50% precision (2σ) either by RVs or TTVs[21]. Previous studies of small planets from the prime *Kepler* mission revealed a transition in the typical composition of planets from mostly rocky to planets having thick envelopes of low density H/He at $\approx 1.6\,R_\oplus$ (Weiss & Marcy 2014; Marcy et al. 2014; Lopez & Fortney 2014; Rogers 2015; Dressing et al. 2015). An important open question is if and how this transition depends on incident stellar flux. Jontof-Hutter et al. (2016) illustrate that the population of planets $< 30\,M_\oplus$ tend to have fewer volatiles as incident flux increases, consistent with atmospheric loss via photoevaporation. WASP-47e is among the most highly irradiated small planets with a well-measured mass, and thus helps us to probe the mass-radius relationship at extreme values of incident stellar flux, in a regime similar to Kepler-10b, Kepler-78b, and 55 Cnc e.

The measured mass of WASP-47e ($9.11 \pm 1.17\,M_\oplus$) is consistent with the measurement of Dai et al. (2015) ($12.2\pm3.7\,M_\oplus$) at the 1σ level. We improve the fractional uncertainty from 30% to 13%, allowing for a more detailed interpretation of composition. The measurements of Dai et al. (2015) favored an admixture of 50% iron and 50% rock. Assuming an iron-rock admixture, we sample our planet mass and radius posterior distributions and compute an iron mass fraction (IMF) using Equation 8 of Fortney et al. (2007). From 100,000 independent samples, we obtain a median IMF of 13% and a 1σ upper limit of 24%, suggesting that WASP-47e is mostly rock. Its IMF is lower than Earth's IMF (33%) at 80% confidence. Alternatively, WASP-47e could have an IMF similar to Earth but possess a significant atmosphere of a high mean molecular weight species, such as water or sulfur.

The measured mass and radius of WASP-47d ($12.75 \pm 2.70\,M_\oplus$ and $3.71 \pm 0.26\,R_\oplus$) are consistent with several other planets, including Kepler-94b, Kepler-95b, Kepler-30b, KOI-142b, and GJ 3470b. With an incident flux $S_{\mathrm{inc}} = 157\pm23\,S_\oplus$, the atmosphere of WASP-47d might have undergone significant photoevaporation. Nevertheless, it must still have an atmosphere containing some amount of H/He. There are a number of degenerate planet compositions in this region of the mass-radius diagram with different fractions of rock, iron, water, and H/He (Rogers & Seager 2010; Valencia et al. 2013). Possible compositions include a small iron-rich or rocky core with an extended H/He or steam envelope, or a water-world with a modest H/He envelope. Future transmission spectroscopy observations would help to break these degeneracies.
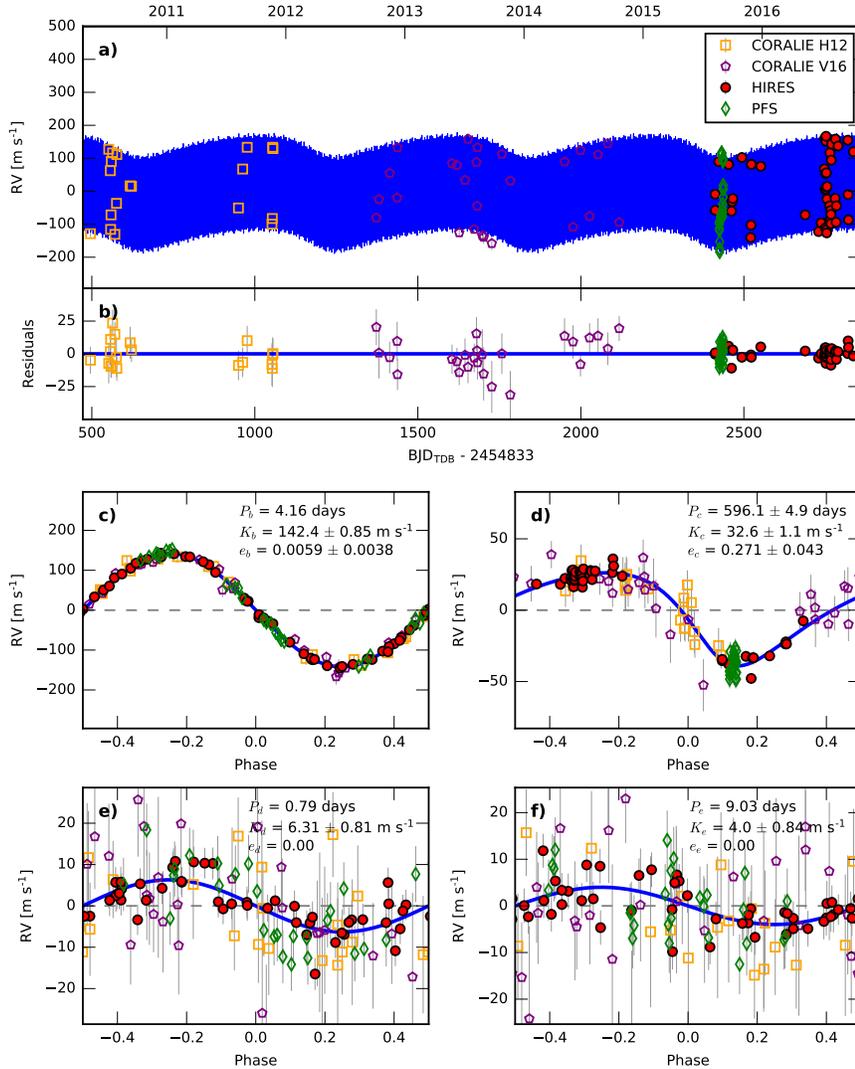
FIG. 1.— Four-planet RV model of WASP-47, assuming circular orbits for WASP-47d and WASP-47e **a)** The RV time-series. Filled red circles indicate Keck-HIRES data. Orange squares represent CORALIE data published by Hellier et al. (2012). Purple pentagons represent CORALIE data published by Neveu-VanMalle et al. (2016). Green diamonds indicate PFS data published by Dai et al. (2015). The solid blue line corresponds to the most likely model. Note that the orbital parameters listed in Table 2 are the median values of the posterior distributions. Error bars for each independent dataset include an RV jitter term listed in Table 2, which are added in quadrature to the measurement uncertainties. **b)** Residuals to the maximum-likelihood fit. **c-f)** The RV time-series phase folded at the orbital periods of each of the four planets after subtracting the other three planet signals.

WASP-47e is among the few known USP planets $> 1.5\,R_\oplus$. Lopez (2016) explains the dearth of larger USP planets as a consequence of photoevaporation of H/He envelopes of larger planets that formed water-poor. The one potential counter-example noted by Lopez (2016) is the $1.9\,R_\oplus$ USP planet 55 Cnc e. The most recent mass and radius constraints suggest the presence of a water-rich envelope, $8 \pm 3\%$ of the planet's mass.

55 Cnc has remarkable similarities to WASP-47. It hosts a USP super-Earth (55 Cnc e), a non-transiting giant planet (55 Cnc b) at P=15 days, and three additional non-transiting planets at $P = 44, 262$, and ~ 4800 days. The fact that these systems host both a HJ and a USP planet suggests that their formations are linked in some way. Moreover, the mass and radius of 55 Cnc e ($8.3 \pm 0.3\,M_\oplus$, $1.92 \pm 0.08\,R_\oplus$) are consistent with

WASP-47e ($9.11 \pm 1.17\,M_\oplus$, $1.87 \pm 0.13\,R_\oplus$). Therefore, both planets could have water-rich envelopes. More well-characterized USP planets $\approx 2\,R_\oplus$ are needed to determine if they represent a distinct population of USP planets spawning from unique formation and/or evolutionary processes. In particular, as proposed by Huang et al. (2016), WASP-47b and 55 Cnc b might represent the rare close-in extremes of in-situ formation hypothesized to produce the $\sim 50\%$ of warm-Jupiters ($P = 10$–200 days) that have small companions at shorter orbital distances. This highlights the limitations of classifying HJs and warm-Jupiters based on orbital period alone, without taking the more complete system architecture into account.

One clue about the formation history of 55 Cnc e is the fact that it transits whereas the outer planet (P

TABLE 2
WASP-47 SYSTEM PARAMETERS

Parameter	Value	Units	Ref.
Stellar Parameters			
$T_{\rm eff}$	5475 ± 60	K	A
$\log g$	4.27 ± 0.05	dex	A
[Fe/H]	0.36 ± 0.05	dex	A
$v \sin i$	$1.80^{+0.24}_{0.16}$	km s^{-1}	C
$M_\star$	0.99 ± 0.05	$M_\odot$	A
$R_\star$	1.18 ± 0.08	$R_\odot$	A
Planet Parameters			
WASP-47b			
P	4.1591287 ± 0.000019	days	A, B
$T_{\rm conj}$	$2457007.932131 \pm 0.000023$	BJD	B
$R_p/R_\star$	0.10186 ± 0.00023	—	B
a	0.05047 ± 0.00085	AU	A
$S_{\rm inc}$	441 ± 65	$S_\oplus$	A
R_p	13.11 ± 0.89	$R_\oplus$	A
e	$0.0036^{+0.0049}_{-0.0026}$	—	A
ω	91^{+183}_{-39}	deg	A
K	142.34 ± 0.85	m s^{-1}	A
M_p	356 ± 12	$M_\oplus$	A
ρ_p	0.87 ± 0.18	g cm^{-3}	A
WASP-47c			
P	595.7 ± 5.0	days	A
$T_{\rm conj}$	2455992 ± 10	BJD	A
a	1.382 ± 0.023	AU	A
$S_{\rm inc}$	0.59 ± 0.09	$S_\oplus$	A
e	0.27 ± 0.04	—	A
ω	136 ± 12	deg	A
K	32.62 ± 1.14	m s^{-1}	A
M_p	411 ± 18	$M_\oplus \sin i$	A
WASP-47d (circular orbit assumed)			
P	9.03081 ± 0.00074	days	A, B
$T_{\rm conj}$	$2457006.36927 \pm 0.00044$	BJD	B
$R_p/R_\star$	0.02886 ± 0.00047	—	B
a	0.0846 ± 0.0014	AU	A
$S_{\rm inc}$	157 ± 23	$S_\oplus$	A
R_p	3.71 ± 0.26	$R_\oplus$	A
K	3.94 ± 0.82	m s^{-1}	A
M_p	12.75 ± 2.70	$M_\oplus$	A
ρ_p	1.36 ± 0.42	g cm^{-3}	A
WASP-47e (circular orbit assumed)			
P	0.789597 ± 0.000013	days	B
$T_{\rm conj}$	$2457011.34849 \pm 0.00038$	BJD	B
$R_p/R_\star$	0.01456 ± 0.00024	—	B
a	0.01667 ± 0.00028	AU	A
$S_{\rm inc}$	4043 ± 593	$S_\oplus$	A
R_p	1.87 ± 0.13	$R_\oplus$	A
K	6.34 ± 0.78	m s^{-1}	A
M_p	9.11 ± 1.17	$M_\oplus$	A
ρ_p	7.63 ± 1.90	g cm^{-3}	A
Other			
$\gamma_{\rm HIRES}$	6.4 ± 1.5	m s^{-1}	A
$\gamma_{\rm PFS,D15}$	20.5 ± 2.9	m s^{-1}	A
$\gamma_{\rm CORALIE,H12}$	-27070.3 ± 5.1	m s^{-1}	A
$\gamma_{\rm CORALIE,V16}$	-27085.3 ± 2.7	m s^{-1}	A
$\sigma_{\rm jit,HIRES}$	3.7 ± 0.6	m s^{-1}	A
$\sigma_{\rm jit,PFS,D15}$	6.3 ± 1.2	m s^{-1}	A
$\sigma_{\rm jit,CORALIE,H12}$	5.9 ± 3.5	m s^{-1}	A
$\sigma_{\rm jit,CORALIE,V16}$	6.7 ± 3.3	m s^{-1}	A

NOTE. — $S_{\rm inc}$ = Incident flux, $T_{\rm conj}$ = Time of conjunction, A: This study, B: Becker et al. (2015), C: Sanchis-Ojeda et al. (2015). H12: Hellier et al. (2012), D15: Dai et al. (2015), V16: Neveu-VanMalle et al. (2016). Orbital periods of planets b and d are those from Becker et al. (2015), but with larger uncertainties (See §3).
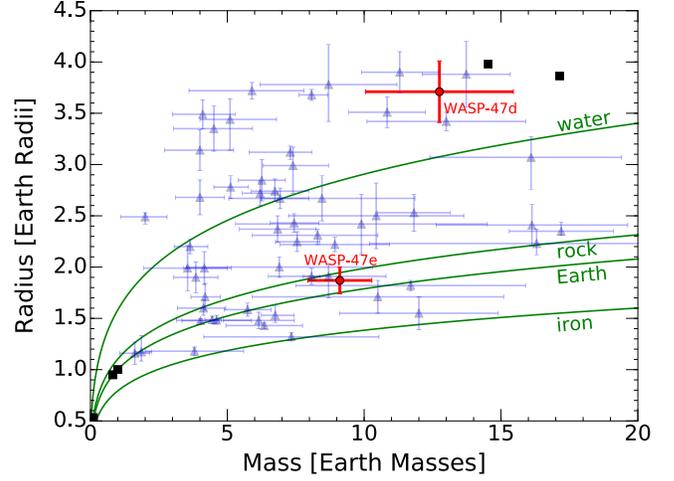

FIG. 2.— Radii and masses of all confirmed planets whose mass and radius are measured to better than 50% (2σ) precision (blue triangles). Solar System planets are represented as black squares. Red circles indicate our measurements of WASP-47d and WASP-47e. Green curves show the expected planet mass-radius curves for 100% iron, 100% rock (Mg_2SiO_4), 100% water (ice), and Earth-like (67% rock, 33% iron) compositions according to models by Fortney et al. (2007).

~4800 days) is claimed, on the basis of HST astrometry, to be inclined to the line of sight by 30 degrees (McArthur et al. 2004). Hansen & Zink (2015) showed that if 55 Cnc e formed slightly beyond its current orbit, and migrated inwards through tidal dissipation, it would have crossed a pair of secular resonances in the system, which could have boosted its inclination and/or eccentricity. This would increase the tidal heating and potentially devolatilize the planet or drive it to Roche lobe overflow. The WASP-47 system also shows a potential secular resonance if WASP-47e once had a semi-major axis of 0.022 AU. Although this system clearly did not experience pumping of the inclination, a small but finite initial eccentricity for WASP-47d could have driven tidal evolution of WASP-47e through this resonance and rapidly increased the tidal heating, potentially leading to strong devolatilization. If WASP-47e and WASP-47d both formed as Neptune-size planets,, but WASP-47e was heated or tidally stripped, then their current difference in densities reflects their evolution rather than their origins.

From our MCMC analysis of the RV time-series, we determine the orbital eccentricity of the HJ to be < 0.021 at 99.7% (3σ) confidence. The very low eccentricity and the alignment between the orbital axis and stellar spin (Sanchis-Ojeda et al. 2015) are consistent with disk migration, in-situ formation, and the aforementioned secular interaction scenario. In future, this eccentricity constraint can be used to inform TTV models.

WASP-47 has a high metallicity (0.36 ± 0.05 dex) which has been shown to be associated with HJ occurrence and giant planet occurrence (e.g. Fischer & Valenti 2005; Buchhave et al. 2014). The Kepler sample of Earth-size planets were found around stars of widely varying metallicity (Buchhave et al. 2014). However, if USPs are associated with metal-rich stars, it suggests different formation pathway than the bulk of known Earth-size planets—one that may be more closely associated with HJs. Although it is beyond the scope of this study, a comparison between the metallicities of stars hosting HJs

with those hosting USPs will provide a useful test of the relationship between the formation of USPs and HJs.

We note that while this manuscript was under review, Almenara et al. (2016) reported mass and radius constraints of the WASP-47 system using a photodynamical model. They simultaneously fit the *K2* photometry and the RV measurements of Hellier et al. (2012), Dai et al. (2015), and Neveu-VanMalle et al. (2016). Their planet mass measurements are consistent with this study at the 1-σ level. Future incorporation of our Keck-HIRES RVs into a photodynamical analysis would further improve constraints of the WASP-47 system.

Facilities: Kepler, Keck-HIRES.

TABLE 3
RELATIVE RADIAL VELOCITIES, KECK-HIRES

BJD	RV [m s^{-1}][a]	Unc. [m s^{-1}][b]	$S_{\rm HK}$
2457244.871067	0.48	1.67	0.126
2457244.878949	5.92	1.77	0.132
2457244.887016	-1.84	1.66	0.133
2457244.895257	-3.04	1.82	0.135
2457244.903486	-1.37	1.64	0.132
2457244.911878	-3.26	1.84	0.127
2457244.920153	-5.65	1.59	0.135
2457244.928510	-8.04	1.76	0.133
2457244.936600	-8.56	1.66	0.135
2457244.944818	-2.06	1.71	0.135
2457244.953082	-0.15	1.66	0.130
2457244.961427	-0.13	1.62	0.132
2457244.969923	-4.30	1.73	0.131
2457244.978731	-9.13	1.77	0.131
2457244.987215	-20.02	1.73	0.130
2457244.995815	-20.64	1.68	0.136
2457245.004993	-29.55	1.73	0.121
2457245.013720	-32.44	1.66	0.127
2457245.022227	-39.56	1.67	0.135
2457245.030607	-39.94	1.59	0.136
2457245.038917	-43.69	1.62	0.104
2457245.047448	-48.47	1.65	0.129
2457245.056198	-53.78	1.52	0.129
2457245.065700	-50.95	1.79	0.114
2457245.074508	-46.85	1.60	0.123
2457245.083096	-44.16	1.65	0.130
2457245.091812	-48.39	1.52	0.133
2457245.100712	-57.42	1.53	0.129
2457245.110018	-52.81	1.68	0.134
2457256.103458	96.66	2.11	0.135
2457286.030224	87.81	2.19	0.089
2457294.949126	-53.43	2.17	0.115
2457296.992830	-24.59	2.00	0.137
2457298.980931	-15.40	3.62	0.131
2457326.879645	108.91	1.96	0.036
2457353.819776	-133.61	2.05	0.142
2457354.803856	-95.88	1.95	0.128
2457355.794764	88.20	1.99	0.127
2457384.711392	82.45	1.93	0.127
2457521.108185	-64.84	1.86	0.126
2457562.108559	-115.52	1.81	0.160
2457570.076758	-89.15	2.05	0.151
2457580.060228	74.59	1.83	0.140
2457581.046494	167.52	1.81	0.131
2457582.043488	12.38	1.98	0.135
2457583.061003	-104.76	1.83	0.136
2457583.922512	13.32	1.83	0.133
2457584.109907	59.97	1.80	0.127
2457584.914664	158.68	1.90	0.137
2457585.068538	173.44	1.79	0.135
2457585.911306	62.57	1.98	0.140
2457586.089591	19.48	2.04	0.127
2457586.909613	-110.17	1.72	0.131
2457587.088454	-119.61	1.67	0.138
2457587.950710	-16.79	2.01	0.136
2457588.097234	21.03	1.80	0.141
2457595.894592	-81.36	2.24	0.138
2457596.120574	-37.76	2.18	0.121
2457596.917828	123.24	2.11	0.131
2457598.938091	-51.78	2.07	0.119
2457599.106292	-79.28	1.95	0.135
2457599.928092	-91.45	1.83	0.140
2457600.118064	-63.52	1.87	0.135
2457600.927270	101.12	2.06	0.138
2457602.055444	149.79	2.09	0.132
2457612.852525	-14.58	1.83	0.136
2457614.023768	164.96	1.77	0.135
2457615.871589	-87.25	1.96	0.132
2457616.894897	-37.49	1.90	0.133
2457622.042983	143.94	2.30	0.129
2457651.804239	161.48	1.74	0.128
2457652.803402	-3.55	1.77	0.145
2457653.938888	-80.03	1.86	0.142
2457668.749161	126.48	2.14	0.143

[a] RVs do not include zero point offset ($\gamma_{\rm HIRES}$, Table 2)
[b] Uncertainties do not include jitter ($\sigma_{\rm jit,HIRES}$, Table 2)

REFERENCES

Almenara, J. M., Díaz, R. F., Bonfils, X., & Udry, S. 2016, A&A, 595, L5

Batygin, K., Bodenheimer, P. H., & Laughlin, G. P. 2016, ApJ, 829, 114

Becker, J. C., Vanderburg, A., Adams, F. C., Rappaport, S. A., & Schwengeler, H. M. 2015, ApJ, 812, L18

Brewer, J. M., Fischer, D. A., Basu, S., Valenti, J. A., & Piskunov, N. 2015, ApJ, 805, 126

Brewer, J. M., Fischer, D. A., Valenti, J. A., & Piskunov, N. 2016, ApJS, 225, 32

Buchhave, L. A., Bizzarro, M., Latham, D. W., et al. 2014, Nature, 509, 593

Burke, C. J., Christiansen, J. L., Mullally, F., et al. 2015, ApJ, 809, 8

Butler, R. P., Marcy, G. W., Williams, E., et al. 1996, PASP, 108, 500

Crossfield, I. J. M., Ciardi, D. R., Petigura, E. A., et al. 2016, ApJS, 226, 7

Dai, F., Winn, J. N., Arriagada, P., et al. 2015, ApJ, 813, L9

Dawson, R. I., Murray-Clay, R. A., & Johnson, J. A. 2015, ApJ, 798, 66

Deck, K. M., Agol, E., Holman, M. J., & Nesvorný, D. 2014, ApJ, 787, 132

Dotter, A., Chaboyer, B., Jevremović, D., et al. 2008, ApJS, 178, 89

Dressing, C. D., Charbonneau, D., Dumusque, X., et al. 2015, ApJ, 800, 135

Feiden, G. A., & Chaboyer, B. 2012, ApJ, 757, 42

Fischer, D. A., & Valenti, J. 2005, ApJ, 622, 1102

Ford, E. B. 2006, ApJ, 642, 505

Foreman-Mackey, D., Hogg, D. W., Lang, D., & Goodman, J. 2013, PASP, 125, 306

Fortney, J. J., Marley, M. S., & Barnes, J. W. 2007, ApJ, 659, 1661

Fressin, F., Torres, G., Charbonneau, D., et al. 2013, ApJ, 766, 81

Gelman, A., & Rubin, D. B. 1992, Statist. Sci., 7, 457

Hansen, B. M. S., & Zink, J. 2015, MNRAS, 450, 4505

Hellier, C., Anderson, D. R., Collier Cameron, A., et al. 2012, MNRAS, 426, 739

Howard, A. W., Johnson, J. A., Marcy, G. W., et al. 2009, ApJ, 696, 75

—. 2010, ApJ, 721, 1467

Howard, A. W., Marcy, G. W., Bryson, S. T., et al. 2012, ApJS, 201, 15

Howard, A. W., Marcy, G. W., Fischer, D. A., et al. 2014, ApJ, 794, 51

Howell, S. B., Sobeck, C., Haas, M., et al. 2014, PASP, 126, 398

Huang, C., Wu, Y., & Triaud, A. H. M. J. 2016, ApJ, 825, 98

Isaacson, H., & Fischer, D. 2010, ApJ, 725, 875

Jontof-Hutter, D., Ford, E. B., Rowe, J. F., et al. 2016, ApJ, 820, 39

Knutson, H. A., Fulton, B. J., Montet, B. T., et al. 2014, ApJ, 785, 126

Lin, D. N. C., Bodenheimer, P., & Richardson, D. C. 1996, Nature, 380, 606

Lithwick, Y., Xie, J., & Wu, Y. 2012, ApJ, 761, 122

Lopez, E. D. 2016, arXiv:1610.01170, arXiv:1610.01170

Lopez, E. D., & Fortney, J. J. 2014, ApJ, 792, 1

Lucy, L. B., & Sweeney, M. A. 1971, AJ, 76, 544

Marcy, G. W., & Butler, R. P. 1992, PASP, 104, 270

Marcy, G. W., Isaacson, H., Howard, A. W., et al. 2014, ApJS, 210, 20

McArthur, B. E., Endl, M., Cochran, W. D., et al. 2004, ApJ, 614, L81

Mortier, A., Santos, N. C., Sousa, S. G., et al. 2013, A&A, 558, A106

Morton, T. D. 2015, isochrones: Stellar model grid package, Astrophysics Source Code Library, ascl:1503.010

Naoz, S., Farr, W. M., Lithwick, Y., Rasio, F. A., & Teyssandier, J. 2011, Nature, 473, 187

Neveu-VanMalle, M., Queloz, D., Anderson, D. R., et al. 2016, A&A, 586, A93

Petigura, E. A., Marcy, G. W., & Howard, A. W. 2013, ApJ, 770, 69

Powell, M. J. D. 1964, The Computer Journal, 7, 155

Rasio, F. A., & Ford, E. B. 1996, Science, 274, 954

Rogers, L. A. 2015, ApJ, 801, 41

Rogers, L. A., & Seager, S. 2010, ApJ, 712, 974

Sanchis-Ojeda, R., Winn, J. N., Dai, F., et al. 2015, ApJ, 812, L11

Schlaufman, K. C., & Winn, J. N. 2016, ApJ, 825, 62

Sinukoff, E., Howard, A. W., Petigura, E. A., et al. 2016, ApJ, 827, 78

Socrates, A., Katz, B., Dong, S., & Tremaine, S. 2012, ApJ, 750, 106

Steffen, J. H., Ragozzine, D., Fabrycky, D. C., et al. 2012, Proceedings of the National Academy of Science, 109, 7982

Valencia, D., Guillot, T., Parmentier, V., & Freedman, R. S. 2013, ApJ, 775, 10

Valenti, J. A., Butler, R. P., & Marcy, G. W. 1995, PASP, 107, 966

Vogt, S. S., Allen, S. L., Bigelow, B. C., et al. 1994, in Society of Photo-Optical Instrumentation Engineers (SPIE) Conference Series, Vol. 2198, Instrumentation in Astronomy VIII, ed. D. L. Crawford & E. R. Craine, 362

Weiss, L. M., & Marcy, G. W. 2014, ApJ, 783, L6

Wright, J. T., Marcy, G. W., Howard, A. W., et al. 2012, ApJ, 753, 160

Wu, Y., & Lithwick, Y. 2011, ApJ, 735, 109

Wu, Y., & Murray, N. 2003, ApJ, 589, 605